Theoretical prediction of the peak structure in the EELS spectrum of palladium

Gregor-Martin Fehrenbach
Sektion Physik der Ludwig Maximilians Universität München, Theresienstraße 37, 80333 Munich, Germany
(Received 24 October 1997; revised manuscript received 19 January 1999)

The electron-energy-loss spectrum (EELS) of palladium is calculated using an all-electron method within the time-dependent density-functional framework. The band-structure is calculated with the spline augmented plane-wave method that generates a very large number of unoccupied Kohn-Sham levels, which are shown to be necessary for the evaluation of the density response. The exchange-correlation interaction correction is included in the local and static approximation and a mixed basis representation is used for the calculation of the inverse dielectric function. Combining these techniques, it can be shown that the theoretical EELS of palladium is in much better agreement with the experiment than previous all-electron investigations suggested. Especially the peak structure at 0.6 Ry compares now fairly well with experimental results. [S0163-1829(99)03923-5]

I. INTRODUCTION

The dynamic properties of crystal electrons are described essentially by the dielectric function (DEF), since it connects the external fields applied to a system with the response of the system itself. It is well known that the knowledge of the dielectric function is sufficient to calculate the ground-state energy of the many-electron system[1] as well as the quasiparticle corrections to the one-particle energies,[2,3] e.g., within the so-called *GW* approximation. Additionally, the quantities derived from the DEF, e.g., the dynamical structure factor or the electron-energy-loss spectrum (EELS) addressed in this work, are essential for the comparison between experiment and theory.[4,5] However, for two reasons beyond the numerical effort described below, the calculation of the DEF in crystals is a rather demanding task, when compared with a ground-state calculation or with the calculation of optical properties in homogeneous systems or in atoms: First, the periodic structure causes so-called crystal local-field effects, i.e., an external perturbation of momenta $\mathbf{q}$ causes microscopic fields of momentum $\mathbf{q}+\mathbf{G}$, where $\mathbf{G}$ is an arbitrary reciprocal-lattice vector.[6–8] As an immediate consequence, the calculation of the inverse DEF, which describes the EELS spectrum, requires, e.g., the inversion of a matrix of infinite dimension, indexed with reciprocal-lattice vectors $\mathbf{G}$ and $\mathbf{G}'$. In the present calculation, however, we will use a different technique to obtain the inverse DEF, which is discussed in detail below. Second, many-body corrections in crystals have a more complicated form than they have in homogeneous systems. In the latter case, they can simply be discussed in terms of the dynamical generalization of Hubbard's many-body local-field correction factor $G^{hom}(\mathbf{q},\omega)$,[9] to be distinguished from the above-mentioned crystal local-field effects. Therefore, for a rather long time, many calculations of the DEF in crystals were done within the picture of independent Bloch electrons, and often even neglecting crystal local-field corrections. Most calculations used either empirical potentials or, without further justification, the effective Kohn-Sham (KS) potential of ground-state calculations performed within density-functional theory (DFT). While the first choice is without any theoretical foundation, the second choice suffers from the deficiency that it is not possible to interpret the energies of the KS orbitals as one-particle excitations. In this context, the time-dependent local-density approximation (TDLDA), developed by several authors,[10–13] explains only how to use the KS orbitals in the static limit. The calculation of the frequency- and wave-vector-dependent DEF matrix, even at this simple level, requires an amount of numerical work, larger by roughly one order of magnitude than for a corresponding ground-state calculation. This corresponds to the large amount of information which is contained in the DEF. Technically, the increase of numerical effort arises due to the fact that, first, not only the occupied, but all bands are needed. Indeed, as we will show below, quite a large number of bands is necessary to obtain well converged results, at least much more than obtained by many linear band-structure calculations. Second, the calculation of the corresponding matrix elements is quite involved in an all-electron framework. Third, there is a large number of possible transitions, which are to be included in the $\mathbf{k}$ integration. Calculation techniques for the DEF in an all-electron framework has been the subject of theoretical studies for two decades now, e.g., in the framework of the Greens-function method,[14,15] of the linearized muffin-tin orbital method,[16–18] and of the linear combination of Gaussian orbitals scheme,[19] to mention only a few of them. In this paper we show that, by applying theoretical and numerical concepts, we can overcome shortcomings of older calculation techniques. In detail, we apply the time-dependent density-functional theory for the calculation of the density-density response at an all-electron level, using than 500 conduction bands to carry out the perturbation expansion and an interesting technique for the inversion of the DEF. Thereby we are able to reduce the discrepancies between experiment and theory significantly, which show up in previous all-electron investigations on transition metals. We have chosen the EELS spectrum of Pd as a typical example here, since the EELS peak structure around 0.6 Ry was described rather poorly by previous all-electron calculations. Similar deviations between experiment an theory can be found in the EELS spectra of V, Nb, Cr, Mo, and Ru. In all these cases previous theoretical EELS calculations predict sharp plasmon peaks, which either cor-

respond to rather broad humps in the experimental data, or which are even absent. More details can be found in Ref. 20 and the references therein. In this work of Mazin *et al.*, the optical properties of Pd are analyzed on a self-consistent and all-electron level. Earlier investigations of the optical properties of Pd (Refs. 21–26) use empirical one-particle potentials and deal at most with the imaginary part of the DEF in a small frequency range and did not calculate the EELS. While Ray, Chowdhuri, and Chatterjee[21] and Christensen[22] include matrix elements, the other authors[23–26] analyze the optical properties on the level of the combined density of states only.

The remainder of the paper is organized as follows: Sec. II describes the theoretical and numerical concepts used, in Sec. III we discuss the results for the EELS of palladium, and we draw conclusions in Sec. IV.

Complementary to this paper we will present results for the electron-test-charge DEF elsewhere.[27]

II. GENERAL THEORY AND NUMERICAL TECHNIQUES

A. The electron-electron DEF in time-dependent density-functional theory

For roughly a decade, the development of the TDDFT (Refs. 28–30) has been providing a rigorous foundation for calculations of time-dependent quantities in a DFT framework by establishing a set of effective self-consistent, time-dependent one-particle KS equations. This theory generalizes the TDLDA for the dynamic and, at least in principle, nonlocal case. In particular, by working out first-order perturbation theory within TDDFT, the electron-electron dielectric function ϵ reads[30]

$$\underline{\underline{\epsilon}}(\mathbf{q},\omega)=\underline{\underline{1}}-[\underline{\underline{V}}^{C}(\mathbf{q})+\underline{\underline{F}}^{XC}(\mathbf{q},\omega)]\cdot\underline{\underline{\chi}}^{KS}(\mathbf{q},\omega). \tag{1}$$

By its definition, this DEF describes the response of the effective one-particle KS potential felt by the electrons under the influence of an external electronic perturbation. Hence it is the proper dielectric function to discuss EELS spectra. In addition, the DEF (1) describes the screening of the electron-electron interaction used in quasiparticle calculations, e.g., at the GW level.[31] All doubly underlined quantities in Eq. (1) correspond to two-point functions which are integral kernels in coordinate space. For the sake of simplicity, we have used Fourier coefficients so far, e.g.,

$$\begin{aligned}\underline{\underline{\epsilon}}(\mathbf{q},\omega)&=\mathcal{F}[\epsilon(\mathbf{r},\mathbf{r}',\omega)]\\&=\frac{1}{\Omega}\int_{R^6}e^{-i(\mathbf{q}+\mathbf{G})\cdot\mathbf{r}}\epsilon(\mathbf{r},\mathbf{r}',\omega)e^{i(\mathbf{q}+\mathbf{G}')\cdot\mathbf{r}'}d^3r\,d^3r'\end{aligned} \tag{2}$$

to write down Eq. (1), which are understood to be matrices of infinite rank indexed with reciprocal-lattice vectors in the usual Toeplitz sense. Ω is the volume of the unit cell. In the numerical calculations discussed below, however, we are going to use a different representation for the two-point functions. In Eq. (1) V^C is the Coulomb interaction and $\mathcal{X}^{KS}$ is the density-density response function of the time-independent KS ground state of the system

$$\begin{aligned}\mathcal{X}^{KS}_{\mathbf{G},\mathbf{G}'}=\frac{1}{\Omega}\sum_{n,n'}\int d^3k\frac{f_{n\mathbf{k}}-f_{n'\mathbf{k}+\mathbf{q}}}{E_{n\mathbf{k}}-E_{n'\mathbf{k}+\mathbf{q}}+\omega}\\\times\mathcal{P}_{n,n'}(\mathbf{q}+\mathbf{G},\mathbf{k})\mathcal{P}^{*}_{n,n'}(\mathbf{q}+\mathbf{G}',\mathbf{k}),\end{aligned} \tag{3}$$

which is an analytic function of ω in the upper half of the complex ω plane. The $E_{n\mathbf{k}}$ denote the eigenvalues of the static KS equations, the $f_{n\mathbf{k}}$ are the corresponding occupation numbers, and $\mathcal{P}_{n,n'}(\mathbf{q}+\mathbf{G},\mathbf{k})$ are the matrix elements of the density operator

$$\begin{aligned}\mathcal{P}_{n,n'}(\mathbf{q}+\mathbf{G},\mathbf{k})&=\langle n\mathbf{k}|\boldsymbol{\rho}(\mathbf{q}+\mathbf{G})|n'\mathbf{k}+\mathbf{q}\rangle\\&\overset{\mathbf{q}+\mathbf{G}\to 0}{\to}\frac{\mathbf{q}}{2}\cdot\frac{\langle n\mathbf{k}|\boldsymbol{p}|n'\mathbf{k}\rangle}{E_{n\mathbf{k}}-E_{n'\mathbf{k}}};\quad E_{n\mathbf{k}}\neq E_{n'\mathbf{k}},\end{aligned} \tag{4}$$

which, as shown in the second line, can be reduced to matrix elements of the dipole operator in the long-wave limit. Finally, F^{XC} denotes the exchange-correlation interaction correction to the Coulomb potential, which is the Fourier transform of the second functional derivative of the exchange-correlation energy of the system

$$\underline{\underline{F}}^{XC}(\mathbf{q},\omega)=\mathcal{F}\left(\frac{\delta^2E_{XC}}{\delta\rho(\mathbf{r},t)\,\delta\rho(\mathbf{r}',t')}\right). \tag{5}$$

The appearance of this quantity is an important feature of the TDDFT and represents the dynamic and nonlocal generalization of the static derivative $dV^{XC}/d\rho$ of the local exchange and correlation potential, which has been derived earlier in the TDLDA. For further details of the TDDFT formalism we refer to Refs. 29 and 30. When comparing Eqs. (1) and (3) with the corresponding expressions of a system of noninteracting Bloch electrons, one discovers, first of all, that it is now well justified to use the energies and eigenstates of the KS ground state to set up Eq. (3). The deficit connected with the interpretation of the KS energies as excitation energies is removed by the exchange-correlation correction which is to be added to the Coulomb interaction. Second, $\mathcal{X}^{KS}$ describes the density-density response on the level of the effective KS system rather than the actual density response of the interacting many-electron system. The knowledge of the latter is not important for the the calculation of the EELS, which is already described by the response of effective KS potential. However, the response of the many-electron system enters the so-called electron test-charge DEF, which describes the response to external photons. Since we present results for the electron test-charge dielectric function elsewhere,[27] no further discussion of this function is given here.

In the following paragraphs we describe the numerical and analytical aspects of the calculation of the EELS. In detail, the calculation requires: (i) The self-consistent calculation of the band structure; (ii) a summation over the entire spectrum to obtain Eq. (3) in the long-wave limit; (iii) an integration over the Brillouin zone; (iv) the approximation of the exchange-correlation correction to the Coulomb interaction; (v) the inversion of the DEF.

B. Band calculation and evaluation of the KS response

In contrast to a calculation of ground-state properties, the band calculation for the DEF or EELS requires not only the calculation of the occupied but also of all unoccupied bands. The calculation of the band structure is carried out with the spline augmented plane-wave (SAPW) method,[32,33] developed by the author. This all-electron, full-potential scheme uses a mixed basis as trial functions, which consists of plane waves, to guarantee the Bloch boundary conditions, and of localized spline orbitals, to describe the rapid oscillations of the wave function near the atomic sites. The corresponding ansatz for the Bloch states reads in the zeroth unit cell

$$|n\mathbf{k}\rangle = \sum_{|\mathbf{k}_j| \leqslant q} A_j |\mathbf{k}_j\rangle + \sum_{sL} A_{sL} |sL\rangle. \tag{6}$$

Here we restrict ourselves to the case of one atom in the basis, the A's are the variational parameters, $\langle \mathbf{r}|\mathbf{k}_j\rangle = e^{i\mathbf{k}_j\cdot\mathbf{r}}$ denote plane waves with $\mathbf{k}_j = \mathbf{k} + \mathbf{G}_j$, and $\langle \mathbf{r}|sL\rangle = C(ir)^l Y_L(\hat{r}) B_{s\not l}(r)$ are the spline orbitals. In the latter, C is a normalization constant, Y_L a spherical harmonic, $L = (l,m)$, and B_{sl} a B spline as defined in Ref. 32, which vanishes including its first derivative at the boundary of nonoverlapping spheres centered at the atomic sites and outside of all of them. Furthermore, the sums over L in the second term of Eq. (6) run only over those angular momenta which are included in the augmentation and s numbers the B splines. For details of the self-consistent full-potential SAPW scheme we refer to Ref. 33. In the case of palladium, a convergence of 0.1 mRy for the valence bands and the low-lying conduction bands can be guaranteed by using the following set of trial functions: About 90 plane waves, corresponding to an energy cutoff of $q^2 = 13.92$ Ry, 65 s, 33 p, 33 d, and 17 f functions. It is necessary to include f functions in a calculation of the DEF, since the $\mathbf{p}$ operator in Eq. (4) obeys the selection rule $\Delta l = l \pm 1$ and generates transition from the d-type valence bands into f-type conduction bands. The corresponding rank of the eigenvalue problem is about 560. Nonspherical potential contributions are included up to $l = 8$, and 60 $\mathbf{k}$ points in the irreducible wedge are used for the integration over the first Brillouin zone. Correlation was treated within LDA using the Perdew-Zunger[34] parametrization of the Ceperly-Alder[35] results. It is essential for the following discussion that all bands, including the $1s$ core state as well as high-lying conduction bands, are obtained as solution of only one linear eigenvalue problem:

$$(\underline{\underline{H}} - E_{n\mathbf{k}} \underline{\underline{O}}) \cdot \underline{A} = 0, \tag{7}$$

where $\underline{\underline{H}}$ and $\underline{\underline{O}}$ denote the matrices of the Hamiltonian and the overlap, respectively, set up with the SAPW basis functions, and the variational parameters A_j and A_{sL} are arranged linearly in the array $\underline{A}$. Among others, the properties of the SAPW method which are important in the calculation of response functions are: (i) Because the SAPW scheme is strictly linear, all states are mutually orthogonal exactly, despite of how large their energy difference is. (ii) the SAPW wave function has continuous first derivative everywhere. (iii) The basis set of the SAPW ansatz is numerically complete as is explained below.

TABLE I. Comparison of the l.h.s. and r.h.s. of Eq. (8) for three different limits M of the sum over unoccupied bands. The results are given for the (1,3) component, at $\mathbf{k} = (2/pi)/a(0.75,0.25,0.25)$, and for the six highest valence bands. $N_{\max} = 559$ is the number of bands generated by the SAPW ansatz at this $\mathbf{k}$ point. Bands are labeled beginning with the $1s$ state.

n	L.h.s. (exact)	R.h.s. $M = 120$	R.h.s. $M = 300$	R.h.s. $M = N_{\max}$
19	−1.007	−1.027	−1.007	−1.007
20	−0.410	−0.409	−0.410	−0.410
21	2.093	2.094	2.115	2.094
22	0.111	0.176	0.112	0.110
23	0.711	0.632	0.705	0.710

These properties now allow a proper evaluation of the KS-response function: The strict orthogonality and continuous first derivative supports a straightforward application of perturbation theory, used to set up Eq. (1), and calculation of the matrix elements of $\mathbf{p}$, respectively. Moreover, using the methods described in Appendix A of Ref. 32, all integrals with SAPW basis functions can be done analytically. On top of that, the basis set of the SAPW scheme allows us to perform the sum over the unoccupied levels in Eq. (3) properly. The latter turns out to be the most crucial point in a calculation of the DEF. Although Pd is an elementary metal which possesses a relatively simple electronic structure, it is necessary to include more than 300 empty bands in the sum in Eq. (3) to obtain results which are converged within 1%. About half of the contribution of the unoccupied levels were due to transitions into the 30 lowest conduction bands, while all other bands were responsible for the remainder of the sum, and the convergence was very slow. To explain this surprisingly slow convergence in detail, we first note that the convergence behavior of the right-hand side (r.h.s.) of Eq. (3) can be analyzed most easily by a numerical investigation of the generalized f-sum rule of Thomas, Reiche, and Kuhn;[36]

$$m_{ij}^{-1} = 2\delta_{ij} + 8 \sum_{n \neq n'} \frac{\langle n\mathbf{k}|\boldsymbol{p}_i|n'\mathbf{k}\rangle \langle n'\mathbf{k}|\boldsymbol{p}_j|n\mathbf{k}\rangle}{E_{n\mathbf{k}} - E_{n'\mathbf{k}}}, \tag{8}$$

for the tensor of the inverse effective mass. Since the latter can be also calculated directly within a band calculation, this sum rule may be used as a test for the convergence of sums over unoccupied bands. Moreover, by inserting Eq. (4) in Eq. (3) and decomposing the denominators into partial fractions, Eq. (8) can be shown to be of the same order of convergence with respect to the energy denominator as Eq. (3) is for arbitrary frequencies. In Table I we compare the l.h.s. of Eq. (8) for the uppermost valence bands at a typical $\mathbf{k}$ point of Pd with the r.h.s. for differing upper limits M in the sum over unoccupied bands. We have chosen three special values of M: First of all, $M = 120$ corresponding to a band energy of 14.400 Ry above the Fermi level (which roughly corresponds to the plane-wave cutoff), secondly $M = 300$ corresponding to a band energy of 126.46 Ry above the Fermi level and finally all 559 bands generated by the SAPW ansatz at this particular $\mathbf{k}$ point. The latter is the largest possible value for the upper limit of the sum, if the results of a linear band calculation are used. In this case it corresponds to an energy

of about 6×10^5 Ry above the Fermi energy. One would expect that at least 300 bands should be sufficient for an accuracy of about 1%, since the energy denominator for the highest band is larger by at least two orders of magnitude, when compared with the the denominator for the first interband transitions. However, the data in Table I show a different behavior: We first observe, by comparing the first and the fifth columns, that the sum rule (8) is fulfilled within the order of 0.1%, if all bands generated by the SAPW ansatz are included. In addition, these results show, now by comparing columns two to five, that in general more than 300 bands are necessary to achieve convergence of the sum in Eq. (8), and hence in Eq. (3), within 1%. In detail, when we truncate the sum at $M=120$, which is rather a large number of bands for many linear schemes in the case of Pd already, errors between 10 and 30% are to be expected for some bands (here band 22), while this, at a first sight, looks sufficient for other bands (here bands 20 and 21). However, if we increase the upper limit to $M=300$ the result becomes worse for band 21, when compared with the exact value, which shows that the former agreement was purely by chance. Moreover, detailed analysis of the contributions shows that the convergence in Eqs. (3) and (8) is caused mainly by the magnitude of the matrix elements and only to a very small extent due to increasing energy denominators. This explains why the first estimate we gave above was wrong. We conclude from these observations that, to obtain an accuracy of better than 1%, it is necessary to include all bands generated by the SAPW ansatz (6). To understand the slow convergence in Eqs. (3) and (8) from an analytical point of view, we start from the multipole representation of the wave function near the atomic sites. Because of the Coulomb singularity, in the vicinity of the atomic sites the partial wave with angular momentum L takes the form $\langle\mathbf{r}|n\mathbf{k}\rangle\propto r^l Y_L$. Applying the momentum operator gives

$$\langle\mathbf{r}|\boldsymbol{p}_j|n\mathbf{k}\rangle\propto C_1^j l r^{l-1}Y_L+C_2^j r^l Y_{l+1,m'}+C_3^j r^l Y_{l-1,m''}, \quad (9)$$

with constants C_n^j depending on the Cartesian index j. It is now important to recognize that the first two terms of Eq. (9) do not belong to the function space spanned by the entirety of the solutions of the Schrödinger equation and are, therefore, neither supplied by the SAPW ansatz nor by any other band-structure scheme. That is the reason why the expansion of $\langle\mathbf{r}|\boldsymbol{p}_j|n\mathbf{k}\rangle$ into $\langle\mathbf{r}|n\mathbf{k}\rangle$ in general fails at the atomic sites. However, the large variational freedom of the SAPW ansatz, which results from the application of localized spline orbitals instead of less flexible solutions of the radial Schrödinger equation, enables a proper approximation not only of $\langle\mathbf{r}|n\mathbf{k}\rangle$ but also of $\langle\mathbf{r}|\boldsymbol{p}|n\mathbf{k}\rangle$ in a least mean-square sense. This explains the small remaining errors of about 1% between the l.h.s. and the r.h.s. of Eq. (8) we find in Table I in the case of $M=559$. We were able to obtain even smaller errors by increasing the number of spline functions in the SAPW ansatz, which illustrates that the approximation properties of the SAPW ansatz may be improved systematically. Another reason for the good numerical fulfillment of Eq. (8) is the strict orthogonality of all bands generated by the SAPW scheme. The proceeding discussion proves that the unoccupied levels of the KS equations can be used to evaluate perturbation expressions like Eqs. (3) or (8) although there is no physical interpretation connected with the corresponding energies or states. Closing this discussion we remark that the effective masses obtained in DFT here, either by the l.h.s. or the r.h.s. of Eq. (8), can in general not be compared with their experimental counterparts.

Finally, the integration over the Brillouin zone in Eq. (3) is done with 60 special $\mathbf{k}$ points in the irreducible wedge with an improved Gilat-Raubenheimer technique that uses $\nabla_{\mathbf{k}}E_{n\mathbf{k}}$ for interpolation of the energies. Details of this technique are described in Ref. 37 where it was shown to be numerically superior to the tetrahedron method. Additionally, the $\mathbf{k}$ dependence of the denominator of Eq. (3) is linearized.[38] The gradients of the band energies $E_{n\mathbf{k}}$ can be obtained directly by virtue of the Hellmann-Feynman theorem.[39,40] Applied to the linear SAPW eigenvalue problem (7) the theorem states that

$$\nabla_{\mathbf{k}}E_{n\mathbf{k}}=\underline{\underline{A}}^{\dagger}\cdot(\nabla_{\mathbf{k}}\underline{\underline{H}}-E_{n\mathbf{k}}\nabla_{\mathbf{k}}\underline{\underline{O}})\cdot\underline{\underline{A}}, \quad (10)$$

and allows us to calculate $\nabla_{\mathbf{k}}E_{n\mathbf{k}}$ directly from the corresponding gradients of the Hamiltonian $\underline{\underline{H}}$ and the overlap $\underline{\underline{O}}$ multiplied with the corresponding eigenvectors $\underline{\underline{A}}$. Consequently $\nabla_{\mathbf{k}}E_{n\mathbf{k}}$ is obtained within the same accuracy as the eigenvectors. Furthermore, employing the analytical structure of the DEF, we decompose Eq. (3) into its real and imaginary part, either with the aid of Dirac's identity or by adding a small imaginary part to the denominator of Eq. (3), and calculate the corresponding real and imaginary part of the KS response function directly. We found the differences between $\mathrm{Re}\epsilon$ calculated directly and calculated by Kramers-Kronig (KK) integration two orders of magnitude smaller than the sum over the unoccupied levels in the KS response function Eq. (3). Incidentally, it turns out that, compared to the numerical KK integration extending beyond 500 Ry, the direct method for the calculation of the real part of $\mathcal{X}^{KS}$ is the preferable one, since it becomes faster and numerically more accurate. Finally, following Refs. 13 and 41, we separated Eq. (3) into interband and intraband contributions and neglected the intraband contributions to the imaginary part, which have no influence on the EELS in the frequency range we discuss here.

C. Exchange-correlation correction

In contrast to corresponding investigations in atoms,[42] the calculation of the exchange-correlation correction F^{XC} in solids still requires rather crude approximations. In practice, explicit functionals can be obtained either from the local-field correction factor G^{hom} of the homogeneous electron gas or by combining the second functional derivative of the static E_{xc}, with a more or less *ad hoc* treatment of the frequency dependence by a Pade-type parametrization. In crystals, the first approach leads to

$$F^{xc}_{\mathbf{G},\mathbf{G}'}(\mathbf{q},\omega)\approx-\frac{q^2}{4\pi e^2}\delta_{\mathbf{G},\mathbf{G}'}G^{hom}[n](\mathbf{q}+\mathbf{G},\omega), \quad (11)$$

where $G^{hom}[n]$ is the local-field correction factor of the homogeneous electron gas with density n. Available parametrizations of $G^{hom}[n]$ are described extensively in Ref. 43. More recently, $G^{hom}[n]$ was calculated in the static case by Moroni, Ceperley, and Senatore[44] using quantum Monte

Carlo techniques. Equation (11) possesses a full $\mathbf{q}$ and ω dependence, but, unfortunately, it neglects crystal local-field effects in F^{XC} completely. Another peculiarity of all F^{XC}'s based on the local-field correction factor is that they are in general not consistent with the exchange-correlation potential used in the underlying ground-state calculation. Thus exchange and correlation effects are treated differently in the zeroth and in the first order of the perturbation expansion. Moreover, since $G^{hom}[n]$ depends on a single density variable n only, it is not clear which density is to be inserted into Eq. (11) in inhomogeneous systems. In contrast, the second approach, in its simplest form, leads to the well-known result

$$F^{xc}_{\mathbf{G},\mathbf{G}'}(\mathbf{q},\omega) \approx \mathcal{F}\left(\frac{\delta V^{XC}[n](\mathbf{r})}{\delta n(\mathbf{r}')}\right)_{\mathbf{G},\mathbf{G}'}, \tag{12}$$

which, in the case that V^{XC} is a local functional of n, recovers the TDLDA. Hence this approach properly accounts for crystal local-field effects and is consistent with the underlying ground-state calculation as well. However, it neglects the $\mathbf{q}$ and ω dependence completely. Also the additional frequency dependence, which can be introduced by replacing the r.h.s. of Eq. (12) with a frequency dependent Padé approximation, proposed by Gross and Kohn,[29] is correct only for $\omega=0$ [where it recovers Eq. (12)] and for $\omega\to\infty$ and interpolates in between. Fortunately, frequency dependence of F^{XC} is not very important, since we find, in accord with other calculations,[45,46] that it is quite small in the range of optical or EELS experiments. We convinced ourselves by intensive test calculations that no significant effects in the EELS are caused by neglecting the time dependence in Eq. (12), while the use of the first approach (11) gave slightly worse results, when compared with the experimental data. However, the most significant changes in the DEF occured via the KS response function, which reacts sensitively to the approximation on the exchange and correlation potential used in the underlying ground-state calculation. This finding first suggests that in general F^{XC} gives a rather small correction to the Coulomb interaction. Second, it emphasizes the requirement that the exchange and correlation correction should be consistent with the particular V^{XC} used in the ground-state calculation. This can be achieved most easily by employing Eq. (12) the frequency-dependent generalization of which did not change the results visibly. Therefore in transition metals, the TDLDA seems to give a sufficient description of the exchange-correlation correction in comparison with other available techniques. However, the various deficiencies of the approximations (11) and (12) show that there is need for more realistic approximation on F^{XC}.

D. Inversion of the DEF

It is well known that the EELS spectrum calculated within first Born approximation[47] $\sigma_{EELS}(\omega)$ is related to the DEF in the long-wave limit via

$$\sigma_{EELS}(\omega) = -\operatorname{Im}\epsilon^{-1}_{\mathbf{0},\mathbf{0}}(\mathbf{0},\omega). \tag{13}$$

Therefore it is necessary to calculate the inverse function of Eq. (1). For any two-point function Z (like ϵ, $\mathcal{X}^{KS}$, V^C, or F^{XC}) the inverse is in general defined in coordinate space by

$$\delta(\mathbf{r}-\mathbf{r}') = \int Z^{-1}(\mathbf{r},\mathbf{r}'')Z(\mathbf{r}'',\mathbf{r}')d^3r'', \tag{14}$$

where, here and for the remainder of this paragraph, the frequency arguments of the two-point functions are omitted. In general, Eq. (14) is an integral equation for Z^{-1}, and approximate solutions on it can be obtained most easily within a suitably chosen finite-dimensioned representation. In solid-state physics the plane-wave representations of two-point functions

$$Z(\mathbf{r},\mathbf{r}') = \frac{\Omega}{(2\pi)^3}\sum_{\mathbf{G},\mathbf{G}'}\int e^{i(\mathbf{q}+\mathbf{G})\mathbf{r}}Z_{\mathbf{G},\mathbf{G}'}(\mathbf{q})e^{-i(\mathbf{q}+\mathbf{G}')\cdot\mathbf{r}}d^3q \tag{15}$$

by its Fourier coefficients $Z_{\mathbf{G},\mathbf{G}'}(\mathbf{q})$, as employed above in Eqs. (1)–(5), is mostly used. Within this representation the matrix of the plane-wave coefficients of the corresponding inverse function is the inverse of the matrix $\underline{\underline{Z}}$, if $\underline{\underline{Z}}$ is indexed with reciprocal-lattice vectors in the usual Toeplitz form. To this end, all matrices of plane-wave coefficients of two-point functions in Eqs. (1)–(5) have infinite rank, and must be truncated at a particular reciprocal-lattice vector in any practical calculation. To judge the numerical capability of a certain representation, we require that Eq. (3) must be able to describe the polarization of the KS system caused by an external perturbation properly. In an all-electron framework, the induced electron charge is not only influenced by the weak external perturbation, but also by the rigid lattice of point charges, and therefore will show oscillating behavior, too. For this reason, the plane-wave representation (15) cannot be expected to converge very fast. Consequently, a large number of reciprocal-lattice vectors must be included in the matrices of the Fourier coefficients to obtain well converged results for the corresponding inverse matrix. The slow convergence is caused by redistributions of the localized inner-shell electrons. Since an all-electron calculation should be able to handle delocalized electrons as well as states localized near the atomic sites, an expansion of ϵ and $\mathcal{X}^{KS}$ into a mixed basis of plane waves and localized functions looks superior to the pure plane-wave representation (12). Therefore we employed the expansion of a two-point function Z into an arbitrary (not necessarily orthogonal) basis of Bloch functions $\{|j\mathbf{q}\rangle\}$:

$$Z(\mathbf{r},\mathbf{r}') = \frac{\Omega}{(2\pi)^3}\sum_{j,j'}\int \langle\mathbf{r}|j\mathbf{q}\rangle Z_{j,j'}(\mathbf{q})\langle j'\mathbf{q}|\mathbf{r}'\rangle d^3q. \tag{16}$$

In the case when the Bloch functions $|j\mathbf{q}\rangle$ are chosen mutually orthogonal Eq. (16) recovers the well-known biorthogonal expansion,[48] for which simple formulas for the coefficients $Z_{j,j'}(\mathbf{q})$ can be obtained. However, in the current calculation it was convenient to choose ansatz functions similar to those of the SAPW ansatz (3), which have nonvanishing overlap. In detail, we use a mixed basis, similar to the basis of the SAPW ansatz (6). It consists of $\mathcal{N}_{pmx}=27$ plane waves (for which $|j\mathbf{q}\rangle=|\mathbf{q}_k\rangle$) and of localized B splines with s symmetry, [for which $|j\mathbf{q}\rangle=|s(0,0)\rangle$]. Thereby five B splines turned out to be sufficient. As a consequence of the long-wave limit the number $\mathcal{N}_{\max}$, which is

necessary to represent ϵ and χ^{KS}, can be chosen about one magnitude smaller than the rank $N_{\max}$ of the eigenvalue problem of the band calculation. Since the basis function is used to represent the two-point functions are not mutually orthogonal, the inverse relation to Eq. (16) required to obtain the expansion coefficients is slightly more complicated and involves the inverse of the overlap matrices. Additional rules must be developed for inversion and convolution. Explicit formulas for these operations will be presented by us elsewhere.[27] The special choice of the basis functions enables us to calculate all matrix elements of the density operator with SAPW basis functions analytically in a very simple manner, and it is still possible to interpret the matrix elements between the plane waves in the usual way. From the numerical point of view, Eq. (16) proved itself to be superior to Eq. (15) in the case when the inverse dielectric matrix of Pd was calculated: While we needed about 65 plane waves in Eq. (15) to obtain the EELS within an accuracy of 1% from the corresponding DEF ϵ, the same accuracy can be obtained with the aid of Eq. (16) using 27 plane waves and 5 *B*-spline functions for $\ell=0$. Thereby the numerical cost for the inversion of Eq. (1) was lowered by roughly 25% and we also saved computation time since a smaller number of matrix elements were needed. Additional test calculations showed that corrections, which can be expected when increasing $\mathcal{N}_{pw}$, when including more *s*-type *B* splines, or when including *B* spline functions with higher angular momentum, are in general below 1%.

In addition, in the long-wave limit q^{-1} singularities show up in the elements $\epsilon_{\mathbf{0},\mathbf{G}}$ of the DEF (1) and in the corresponding plane-wave elements when using the representation (16). The analytical properties of ϵ and ϵ^{-1} which result from these singularities were first investigated by Pick and Martin.[49] In case of the RPA, Pick and Martin were able to show that inverse DEF ϵ^{-1} has also q^{-1} singularities in their $(\mathbf{0},\mathbf{G})$ elements and explained how these elements can be handled. It is not too difficult to show, that analogous formulas apply to the DEF in TDDFT when the representation (16) is used, too. In detail, we find

$$\begin{aligned} &Z_{\mathbf{0},\mathbf{G}}(\mathbf{0},\omega)\propto q^{-1}, \\ &Z_{\mathbf{0},j}(\mathbf{0},\omega)\propto q^{-1} \quad (j\text{-spline index}), \\ &Z_{\mathbf{G},\mathbf{0}}(\mathbf{0},\omega)\propto q, \\ &Z_{j,\mathbf{0}}(\mathbf{0},\omega)\propto q \quad (j\text{-spline index}), \end{aligned} \tag{17}$$

where Z now stands for ϵ or ϵ^{-1} while in all other cases

$$Z_{j,j'}(\mathbf{0},\omega)=\text{finite} \tag{18}$$

holds. We treated these singularities numerically with the help of the Hermitian dielectric matrix (HDM) method,[13,50] which was slightly modified for our purposes to apply to the case when the representation (16) is used.

III. RESULTS AND DISCUSSION

Figure 1 compares the EELS calculated in the present work with experimental data of Daniels and co-workers,[51,52] obtained with electron spectroscopy, and with the results of a previous all-electron calculation, which was carried out by Mazin *et al.*[20] within random-phase-approximation (RPA) using a linearized muffin-tin orbital[53,54] (LMTO) scheme to evaluate the band structure. In the latter calculation 16 bands are used to model the valence and conduction-band structure and crystal local-field effects are neglected. While the overall structure is qualitatively the same in all three curves, we discover that the broad peak, which occurs in the experimental data at 0.54 Ry compares quite well with a hump at 0.60 Ry in the present calculation. On the contrary, the results of Maximov *et al.* predict a very narrow peak which is twice as high as the experimental one at 0.61 Ry. Also the features which can be observed in the experimental curve between 1.50 and 2.20 Ry are overestimated by this calculation. Oppositely, the present calculation is in rather close agreement with the experimental data, although it slightly overestimates the EELS between the first and the second peak (1.24 Ry present calculation, 1.23 Ry experiment) while it underestimates it at the third peak (1.80 Ry present calculation, 1.83 Ry experiment) as well as for higher frequencies. Nevertheless, the positions and structures of the second and the third peak agree fairly well with the experimental data and much better than the results of Mazin *et al.* do. The additional structure, which can be seen in both theoretical curves between 0.2 and 0.5 Ry, which is not present in the experimental data, stems from intraband transition around *L* and *W*. Since the Fermi surface is quite complicated in this region (see Ref. 26 for a plot of the Fermi surface of Pd), we expect that these transitions react quite sensitive to further many-body or relativistic corrections, which have been neglected in both calculations. In addition, the relation between the EELS spectrum and the inverse DEF (13) is restricted to the first Born approximation, which is exact for scattering of very fast electrons only. Therefore, to a minor extent, also intrinsic deviations between the EELS and the inverse DEF can be responsible for the discrepancies that show up between experiment and theory. Nevertheless, the overall agreement between our calculation and the experimental results is quite good, while our SAPW calculation and the older LMTO investigation roughly differ by a factor of 2 over a large frequency range.

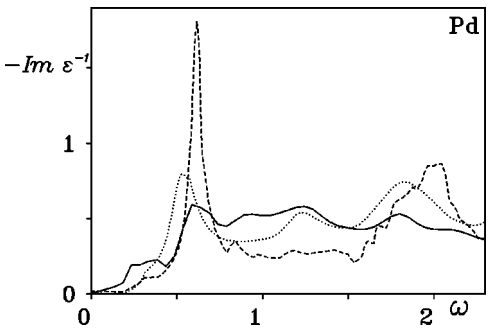

FIG. 1. EELS of solid palladium. Solid line: present work; dashed line: LMTO calculation of Maximov *et al.* (Ref. 20); dotted line: experiment by Daniels and co-workers (Refs. 51 and 52). The energies are in Ry.

To interpret these surprising discrepancies between both calculations we first note that there is an intimate connection between the sharp structure which can be seen in the LMTO results and truncation of the spectrum after only 16 bands.

This connection can be established by remembering the usual *f*-sum rule, which states[47] that

$$\omega_p^2 = -\frac{2}{\pi}\int_0^\infty \omega\, \mathrm{Im}\epsilon^{-1}(0,\omega)d\omega, \tag{19}$$

with the plasma frequency defined by $\omega_p = \sqrt{4\pi n e^2/m}$, where n stands for the number of electrons included in the calculation of ϵ. Since Eq. (19) can be derived from the analytical properties of ϵ^{-1} only, it holds independently from the approximations made for exchange and correlation, if n is set to the number of occupied bands. In turn, deviations from Eq. (19), which occur in numerical calculations are due to the discretization of the **k** integration, the calculation of the response function, and the inversion procedure. Since $\mathrm{Im}\epsilon^{-1}(0,\omega)$ is negative for all frequencies, any truncation of the spectrum of the Hamiltonian by omitting some valence bands will tend to enhance the peaks in the EELS artificially in order to satisfy Eq. (19). This finding shows that even at low frequencies it is necessary to include a large part of the spectrum of the KS equations in the calculation of the DEF in order to describe the structure of the EELS correctly. The high-lying KS levels $|n'\mathbf{k}\rangle$ enter the calculation of $\mathrm{Re}\epsilon$ either directly or via KK integration from $\mathrm{Im}\epsilon$ at the frequencies $E_{n'\mathbf{k}} - E_{n\mathbf{k}} + \omega$, whereby n runs over all occupied bands. As showed above the necessity to include high-lying KS levels is caused by the analytical properties of the dipole operator in presence of a Coulomb singularity. Therefore we expect similar effects to occur also in other response functions. This is supported by the fact that we find Eq. (19) fulfilled within roughly 1% in our calculation.

The other important difference between our calculation and the work of Mazin *et al.*[20] is that crystal local-field effects have been neglected in the latter investigations. In the present work neglecting crystal local-field corrections would have changed the EELS by about 10% in the frequency range shown in Fig. 1 and therefore must be considered to be quite important. However, the error made by neglecting the crystal local-field corrections is small when compared with the error made by using too few unoccupied bands in the evaluation of the KS response. Hence neglecting the crystal local-field corrections can be considered to be only a minor reason for the large deviations between the results of Mazin *et al.*,[20] the experimental EELS, and our results, respectively.

For clarity, we have omitted additional energy-loss data sets published by Weaver and Benbow[55–57] in Fig. 1, since they do not differ too much from the results obtained by Daniels and co-workers.[51,52] In addition, the results of Weaver and Benbow are obtained either by analyzing and and weighing various experimental data,[55,57] which were obtained by several authors and various experimental techniques (e.g., electron as well as photon experiments are employed) or even solely by synchrotron radiation experiments. For details we refer the reader to Ref. 57. As far as photon experiments are concerned it is questionable whether an interpretation in terms of electron-electron DEF is adequate. For these reasons, we believe that the data of Daniels and co-workers[51,52] we used in Fig. 1 are more suited for a comparison with the inverse electron-electron DEF than the data of Weaver and Benbow.

IV. CONCLUSION

The present calculation of the EELS of Pd shows that the differences between an all-electron calculation and the experiment is much smaller than previous theoretical investigations suggested. Our analysis of these results shows that a precise calculation of the KS response function is most important for this improvement and that it requires including a very large number of unoccupied bands in the perturbation expansion of the KS response function. Unfortunately, this increases the computational effort significantly, since the computation time increases like the fourth power of the number of KS levels. There is a faint hope that this effort can be reduced in the future using direct methods to calculate the KS response in an all-electron framework. While such methods for a direct calculation of the KS response function are known for the pseudopotential approximation[58] as well as for spherical atoms,[12] no such techniques are currently applicable to all-electron band-structure methods. In this situation the SAPW method is quite useful, since it is able to generate a number of unoccupied bands, which is large enough to ensure an accurate calculation of the KS response. Beyond this large correction steaming from the use of a numerically complete basis set, only minor improvements can be achieved by including crystal local-field effects and by adding the exchange-correlation correction to the Coulomb interaction.

ACKNOWLEDGMENTS

The author thanks Professor H. Bross for stimulating discussion and the continuous support of his work. He also acknowledges discussions with M. Ehrnsperger and R. Bader as well as with Professor E. K. U. Gross.

[1] L. A. Fetter and J. D. Walecka, *Quantum Theory of Many Particle Systems* (McGraw-Hill, New York, 1971).
[2] L. Hedin, Phys. Rev. **139**, A796 (1965).
[3] R. W. Godby, in *Unoccupied Electronic States*, edited by J. C. Fuggle and J. E. Inglesfield (Springer, Berlin, 1992).
[4] D. Pines and P. Nozières, *The Theory of Quantum Liquids* (New York, Benjamin, 1966).
[5] G. D. Mahan, *Many-Particle Physics* (Plenum, New York, 1981).
[6] H. Ehrenreich and M.L. Cohen, Phys. Rev. **115**, 786 (1959).
[7] S.L. Alder, Phys. Rev. **126**, 413 (1962).
[8] N. Wiser, Phys. Rev. **129**, 62 (1963).
[9] J. Hubbard, Proc. R. Soc. London, Ser. A **243**, 336 (1957).
[10] S.P. Singhal and J. Callaway, Phys. Rev. B **14**, 2347 (1976).
[11] J.F. Dobson and J.H. Rose, J. Phys. C **15**, 7429 (1982).
[12] A. Zangwill and P. Soven, Phys. Rev. A **21**, 1561 (1979).
[13] H. Bross, O.H. Belhachemi, B. Mekki, and A. Seoud, J. Phys.: Condens. Matter **2**, 3919 (1990).
[14] J.F. Janak, A.R. Williams, and V.L. Moruzzi, Phys. Rev. B **11**, 1522 (1975).
[15] A.B. Chen, Phys. Rev. B **49**, 4889 (1976).

[16] Y.A. Uspenskii, E.G. Maximov, S.N. Rashkeyev, and S.N. Mazin, Z. Phys. B **53**, 263 (1983).
[17] M. Alouani, J.M. Koch, and M.A. Kahn, J. Phys. F **16**, 473 (1985).
[18] D. Hobs, E. Piparo, R. Girlanda, and M. Monacca, J. Phys.: Condens. Matter **11**, 1522 (1995).
[19] S.P. Singhal, Phys. Rev. B **14**, 2352 (1976).
[20] I.I. Mazin, E.G. Maksimov, S.N. Rashkeyev, and Y.A. Uspenskii, in *Metal Optics and Superconductivity* (Nova Science, New York, 1991).
[21] P.N. Ray, J. Chowdhuri, and S. Chatterjee, J. Phys. F **12**, 2531 (1982).
[22] N.E. Christensen, Phys. Rev. B **14**, 3446 (1974).
[23] N.V. Smith, Phys. Rev. B **9**, 1365 (1974).
[24] O.K. Andersen, Phys. Rev. B **2**, 883 (1970).
[25] J.F. Janak, D.E. Eastman, and A.R. Williams, Solid State Commun. **8**, 271 (1970).
[26] F.M. Mueller, A.J. Freeman, J.O. Dimmock, and A.M. Furdyna, Phys. Rev. B **1**, 4617 (1970).
[27] G. M. Fehrenbach (unpublished).
[28] E. Runge and E.K.U. Gross, Phys. Rev. Lett. **52**, 997 (1984).
[29] E.K.U. Gross and W. Kohn, Phys. Rev. Lett. **55**, 2850 (1985).
[30] E.K.U. Gross and W. Kohn, in *Density Functional Theory of Many-Fermion Systems*, edited by S.B. Trickey (Academic, New York, 1990).
[31] R. Del Sole, L. Reining, and R.W. Godby, Phys. Rev. B **49**, 8024 (1994).
[32] H. Bross and G.M. Fehrenbach, Z. Phys. B **81**, 233 (1990).
[33] G.M. Fehrenbach and H. Bross, Phys. Rev. B **48**, 17 703 (1993).
[34] J.P. Perdew and A. Zunger, Phys. Rev. B **23**, 5048 (1980).
[35] D.M. Ceperley and B.J. Alder, Phys. Rev. Lett. **45**, 566 (1980).
[36] E. Merzbacher, *Quantum Mechanics* (John Wiley, New York, 1961), p. 446.
[37] H. Bross, Phys. Status Solidi B **179**, 492 (1993).
[38] H. Bross, J. Phys. F **8**, 2631 (1978).
[39] H. Hellmann, *Einführung in die Quantenchemie* (Franz Deutike, Leipzig, 1937).
[40] R.P. Feynman, Phys. Rev. **56**, 340 (1939).
[41] J.E. Sipe and E. Ghahramani, Phys. Rev. B **48**, 11 705 (1993).
[42] M. Petersilka, U.J. Grossmann, and E.K.U. Gross, Phys. Rev. Lett. **76**, 1212 (1996).
[43] B. Dabrowski, Phys. Rev. B **34**, 4989 (1986).
[44] S. Moroni, D.M. Ceperly, and G. Senatore, Phys. Rev. Lett. **75**, 689 (1995).
[45] M. Ehrnsperger and H. Bross, J. Phys.: Condens. Matter **9**, 1225 (1997).
[46] E.K.U. Gross (private communication).
[47] D. Pines, *Elementary Excitations in Solids* (Benjamin, New York, 1964).
[48] P.M. Morse and H. Feshbach, *Methods of Theoretical Physics* (McGraw-Hill, New York, 1953).
[49] R. Pick, M.H. Cohen, and R.M. Martin, Phys. Rev. B **1**, 910 (1970).
[50] S. Baroni and R. Resta, Phys. Rev. B **33**, 7017 (1986).
[51] J. Daniels, Z. Phys. **227**, 234 (1969).
[52] J. Daniels, C. v. Festenberg, H. Raether, and K. Zeppenfeld, in *Optical Constants of Solids by Electron Spectroscopy*, edited by G. Höhler, Springer Tracts in Modern Physics Vol. 54 (Springer, Berlin, 1970), p. 77.
[53] O.K. Andersen, Phys. Rev. B **12**, 3060 (1975).
[54] H.L. Skriver, *The LMTO Method. Muffin-tin Orbitals and Electronic Structure* (Springer, Berlin, 1984).
[55] J.H. Weaver and R.L. Benbow, Phys. Rev. B **12**, 3509 (1975).
[56] J.H. Weaver, Phys. Rev. B **11**, 1416 (1975).
[57] J. H. Weaver, C. Krafka, D. W. Lynch, and E. E. Koch, *Optical Properties of Metals Pt. I: The Transition Metals* (Fachinformationszentrum, Karlsruhe, 1981), Physics Data No.: 18-1.
[58] A.A. Quong and A.G. Eguiluz, Phys. Rev. Lett. **70**, 3955 (1993).